RESEARCH ARTICLE | DECEMBER 09 2024

Nonlinear Bragg resonance of focused wave groups by periodic seabed topography

Qian Wu (吴倩) ; Xingya Feng (冯兴亚) ; You Dong (董优)

Physics of Fluids 36, 127131 (2024)
https://doi.org/10.1063/5.0237127

Physics of Fluids ARTICLE pubs.aip.org/aip/pof

Nonlinear Bragg resonance of focused wave groups by periodic seabed topography

Cite as: Phys. Fluids **36**, 127131 (2024); doi: 10.1063/5.0237127
Submitted: 3 September 2024 · Accepted: 13 November 2024 ·
Published Online: 9 December 2024

Qian Wu (吴倩),[1,2] Xingya Feng (冯兴亚),[2,a)] and You Dong (董优)[1]

AFFILIATIONS

[1]Department of Civil and Environmental Engineering, The Hong Kong Polytechnic University, Hong Kong 999077, China
[2]Department of Ocean Science and Engineering, Southern University of Science and Technology, Shenzhen 518055, China

[a)]Author to whom correspondence should be addressed: fengxy@sustech.edu.cn

ABSTRACT

Bragg resonance induced by periodic bottoms has potential applications for coastal protection. Under extreme wave conditions, nonlinearity may play a critical role in the wave-topography interactions. It is important to understand the nonlinear effects in Bragg resonance of periodic bottoms subject to a nonlinear focused wave group, as a representation of an extreme transient event. An efficient fully nonlinear numerical model using the conformal mapping method is developed to simulate wave-topography interaction problems. Validation of this model is performed against theoretical predictions and experimental data in the literature. It is then employed to study Bragg reflection triggered by nonlinear focused wave groups. The nonlinear analysis finds that increased wave group amplitudes slightly weaken the Bragg reflection and shift the value of the corresponding relative wavelength $2S/L_P$, as a result of the free surface nonlinear effect. The three bottom configurations tested include ripples, rectified cosinoidal bars, and steps. A second order Bragg reflection is observed at $2S/L_P = 2.0$, with reflection coefficients potentially exceeding the fundamental reflection coefficients by up to 20% at greater bar heights. This study provides new insights into the nonlinear Bragg Resonance of free surfaces and periodic seabed topography under extreme wave conditions.

I. INTRODUCTION

Bragg resonance is a wave reflection phenomenon that occurs when the wavelength of submerged bars equals half that of incident waves.[1–3] When the topography is periodic, such as ripples, Bragg resonance can occur at the dimensionless parameter $2S/L = 1, 2, 3\ldots$ (S is the wavelength of sinusoidal bottom undulation), resulting in the reflection of most incoming waves.[4–6] Over the past decade, Bragg resonance has been extensively studied, and five additional types of Bragg resonance have been identified.[7–9] Given the character of large wave reflection, Bragg resonance offers promising applications in coastal protection, such as the use of breakwaters composed of periodic submerged bars to induce Bragg reflection and lessen the effects of extreme waves.[10,11] Therefore, understanding the characteristics of Bragg resonance in coastal engineering is of great significance for the better design of such structures.

Most existing studies have focused on the hydrodynamic performance of submerged bars under regular wave conditions. For instance, Kirby and Anton[12] in 1990 conducted experiments with monochromatic waves propagating over rectified sinusoidal bars, finding reflection coefficients up to 0.7 with a wide bar spacing. The measured data provided a valuable reference for subsequent numerical simulations.[13–16] The Bragg resonance of regular waves over trapezoidal bars was investigated experimentally by Jeon and Cho,[17] reporting reflection coefficients ranging from 0.5 to 0.7 depending on the bar numbers. Miles[18] proposed the theoretical expression for reflection coefficients with monochromatic wave propagation over ripples within the framework of the linear potential flow theory. Recently, Gao *et al.*[19] established a fully nonlinear Boussinesq model (FNBM) for comparison with work by Miles.[18] Apart from regular wave conditions, irregular waves have been examined in several studies.[20–23] The early study by Suh *et al.*[24] utilized a shallow-water spectrum to investigate the Bragg resonance in random waves where both narrow and broad-banded frequency spectra were examined. Subsequently, Hsu *et al.*[22] developed a fully nonlinear model utilizing the second order Boussinesq equations (SFNBE) and corroborated the model with data collected by Davies and Heathershaw,[25] demonstrating reflection coefficients reaching 0.47 for random waves. To sum up, the existing research primarily focuses on either monochromatic or random waves. The interaction between strong nonlinear waves and periodic seabed topography complicates the Bragg resonance studies.

There are limited publications addressing Bragg resonance triggered by large wave groups, which might represent a more realistic

situation in rough sea conditions. In 1993, Liu and Cho[26] verified the long waves associated with the wave groups, which can be reflected resonantly by a field of periodic sandbars. Such a reflection of long waves in the carrier waves was also invested numerically by Cho and Jung[27] in 2006. Gao *et al.*[28] lately investigated the Bragg reflection of irregular wave groups in 2024, after they attempted to mitigate the harbor resonance induced by regular long waves and bi-chromatic short wave groups.[19] Peng *et al.*[7] studied the class III Bragg resonance associated with an incident wave group with a Gaussian envelope in 2019, indicating the influence of Bragg resonance on the evolution of surface wave fields passing over a rippled bottom, especially in the case of shallow water. Given the significance of understanding the hydrodynamic behavior of extreme waves over periodic bars for coastal protection, further investigation into the complex nonlinear wave-topography interactions is needed.

Focused wave groups have been widely employed in the investigation of extreme wave evolution.[29–32] Compared with fundamental Bragg resonance that occurs in the interplay between regular waves and ripples, the higher order Bragg resonance of focused wave groups, which involves complex wave-wave and wave-topography interactions, remains unexplored. Second order Bragg resonance refers to a specific type of resonance phenomenon that occurs when waves interact with periodic structures, such as seabed features, at a higher harmonic frequency.[33] The existing literature on second order Bragg resonance primarily focuses on the interactions of water waves with various artificial seabed structures, such as bars and trenches. Studies by Ding *et al.*[34] in 2024 and Liu[35] in 2023 reported modified Bragg's laws and approximate laws for class I Bragg resonance, while Xie and Liu[16] and Liu *et al.*[36] provided analytical insights into resonances caused by trapezoidal bars on sloping seabeds. However, a notable limitation in this field is the predominance of linear models, which overlook the complexities and nonlinear effects that may significantly influence the resonance behavior in real-world scenarios. Evaluating the nonlinear effects on Bragg resonance with complex bottoms in wave groups needs more advanced approaches.[37] To address this gap, an efficient fully nonlinear numerical model utilizing the conformal mapping method is adopted, capable of handling various types of incident waves and bottom shapes.[38–40]

The primary objective of this study is to investigate the interaction between extreme waves and periodic seabed topography, focusing on the nonlinear Bragg resonance phenomena. By employing a fully nonlinear numerical model, the nonlinear effects of both incident waves and the varying seabed topography on reflection coefficients are discussed. The paper is organized as follows. Section II presents the mathematical formulation of the numerical model and the theoretical expression for the focused wave group. Section III displays the model convergence and validation. Section IV analyzes the nonlinear effects of focused waves and seabed topography. Finally, conclusions and future perspectives are discussed in Sec. V.

II. MATHEMATICAL FORMULATION

A. Fully nonlinear numerical model

A two-dimensional numerical model based on potential flow is developed using the conformal mapping method. The potential flow assumption is based on the fact that the viscous effect is negligible for the problem of wave propagation over a seabed. The fluid is considered inviscid and incompressible, with an irrotational flow. In the fluid domain, the velocity potential $\phi(x, y, t)$ fulfills the Laplace equation.

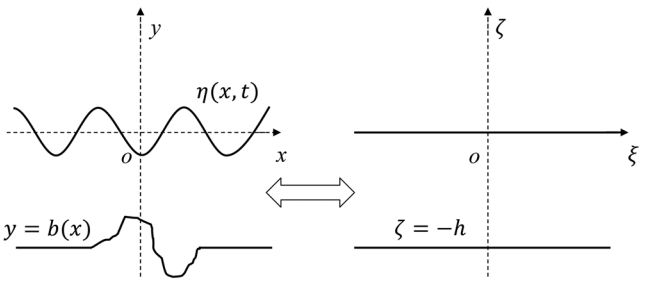

FIG. 1. Transform between the physical domain and the mapped domain.

In the sketch in Fig. 1, the free surface $y = \eta(x, t)$ complies with both kinematic and dynamic boundary conditions. Additionally, the boundary condition at the seabed $y = b(x)$ is required to be impermeable. The governing equation and the boundary conditions are

$$\nabla^2\phi = 0 \quad \text{in} \quad b(x) \le y \le \eta(x, t), \tag{1}$$

$$\eta_t + \phi_x\eta_x - \phi_y = 0 \quad \text{on} \quad y = \eta(x, t), \tag{2}$$

$$\phi_t + \frac{1}{2}\left(\phi_x^2 + \phi_y^2\right) + g\eta = 0 \quad \text{on} \quad y = \eta(x, t), \tag{3}$$

$$\phi_y = 0 \quad \text{on} \quad y = b(x), \tag{4}$$

where the symbol ∇^2 represents the Laplace operator and $\phi(x, y, t)$ denotes the velocity potential in space and time. The subscript denotes the derivative with respect to the variable.

B. Conformal mapping method

In the conformal mapping method, the two-dimensional physical fluid domain (x, y) is determined by the surface profile and the topography. They are then transformed into a mathematical plane (ξ, ζ) defined by two parallel lines, as shown in Fig. 1. The transformation simplifies the solution of the velocity potential in the mapped plane where the upper free surface and lower bottom boundary are fixed. Both boundaries are allowed to be arbitrary in the physical domain, such that any free surface profile and submerged bottom shape can be dealt with.

An analytic function that connects the physical and the mathematical planes can be expressed as $Z = X(\xi, \zeta, t) + iY(\xi, \zeta, t)$. The surface elevation $Y(\xi, 0, t)$ and the topographic profiles $Y(\xi, -h, t)$ can be expressed using the Fourier series:

$$Y(\xi, 0, t) = y(\xi, t) = \sum_{n=-\infty}^{n=\infty} \tilde{Y}_n e^{ink\xi} \quad \text{on} \quad \zeta = 0, \tag{5}$$

$$Y(\xi, -h, t) = b(\xi, t) = \sum_{n=-\infty}^{n=\infty} \tilde{B}_n e^{ink\xi} \quad \text{on} \quad \zeta = -h, \tag{6}$$

where the Fourier coefficients for the surface elevation and the topography are denoted by $\tilde{Y}_n$ and $\tilde{B}_n$, respectively. $i = \sqrt{-1}$ is the imaginary notation and k is the wavenumber. The subscript n is the index of the Fourier terms. The simulation employs the Fourier series to model surface elevation and topographic profiles, utilizing Cauchy–Riemann relations $X_\xi = Y_\zeta$ and $X_\zeta = -Y_\xi$ to derive key expressions. Integral operators are applied to transform variables, facilitating the mapping of governing equations and boundary conditions to a mapped domain.

The original governing equation and boundary conditions Eqs. (1)–(4) for the surface domain variables $x(\xi,0,t)$, $y(\xi,0,t)$, and $\phi(\xi,0,t)$ are transformed into the mapped domain. The governing equations transformed into the mapped domain are

$$x_t - x_\xi\left\{\hbar_m\left[\frac{\psi_\xi}{J},0\right]+q(t)\right\} - y_\xi\left(\frac{\psi_\xi}{J}\right)=0, \tag{7}$$

$$y_t + x_\xi\left(\frac{\psi_\xi}{J}\right) - y_\xi\left\{\hbar_m\left[\frac{\psi_\xi}{J},0\right]+q(t)\right\}=0, \tag{8}$$

$$\phi_t + \frac{1}{J}\left\{\frac{1}{2}(\phi_\xi^2-\psi_\xi^2) - J\phi_\xi\hbar_m\left[\frac{\psi_\xi}{J},0\right]\right\}+gy = C(t), \tag{9}$$

where $J = x_\xi^2 + y_\xi^2$ represents the Jacobian of the free surface profile. The term $C(t)$ is a spatially constant value. The term $q(t)$ is given by $q(t) = m\left\{x_\xi\hbar_m[\frac{\psi_\xi}{J},0] + y_\xi\left(\frac{\psi_\xi}{J}\right)\right\}$. The integral operator $\hbar_m$ implements the interconversion between x_ξ and y_ξ with $x_\xi - 1 = \hbar_m[y_\xi, b_\xi]$ and also affects the system through stream function $\frac{\psi_\xi}{J}$. The operator m denotes the average value of a period. For a detailed examination of the equations and methodologies, please refer to the recent work of Wu *et al.*[40]

To numerically solve the equations in the mapped domain, a pseudo-spectral method is applied. As waves progress over varying seabeds, it is necessary to update the surface elevations $y(\xi,t)$. The objective at each time step is to maintain the conservation condition $y(x(\xi;y(\xi))) = \eta(\xi)$, which requires inverting the conformal mapping through numerical iterations. The fixed-point iterations can be described as follows:

$$y^0 = \eta_0(\xi), \tag{10}$$

$$y^{t+1} = \eta_0(x(\xi;y^t)), \tag{11}$$

where the residual of $|y^{t+1} - y^t|$ should be less than the tolerance of 1×10^{-10} for converged results. The time integration is conducted using an adaptive Adams-Bashforth-Moulton method. This algorithm is distinguished by its stringent error tolerance with a 13^{th}-order formula for error estimation.

C. Generation of focused wave group

The theoretical model of a focused wave group is briefly presented in this study. The focused wave group is a typical wave model used to represent an extreme wave condition, particularly in the experimental studies.[41–43] The wave group is characterized by the sudden appearance of high crests in a short time, similar to features of freak waves in marine environments.[44,45]

The theory of focused wave groups, known as NewWave theory, was proposed by Rapp and Melville[46] in 1990 and is based on the assumption of the superposition of a group of monochromatic waves with aligned phases.[47] The surface elevation and velocity potential of a focused wave group can be expressed as

$$\eta_0(x,t) = \sum_{n=1}^{N} A_n\cos\left[k_n((x-x_{fl}) - c_n(t-t_{fl}))\right], \tag{12}$$

$$\phi_0(x,t) = \sum_{n=1}^{N} A_n c_n \frac{\cosh(k_n h_0)}{\sinh(k_n h_0)}\sin\left[k_n((x-x_{fl}) - c_n(t-t_{fl}))\right], \tag{13}$$

where the focused location x_{fl} and focused time t_{fl} are parameters that set the position and time of maximum wave elevation. The symbol n denotes the nth wave component in the focused wave group. Each wave component is associated with its amplitude A_n, wavenumber k_n, angular frequency ω_n, and phase speed c_n. In this study, the total number of wave components is $N = 2000$, which is sufficiently large. The wave components are generated from a given wave energy spectrum. The standard JONSWAP spectrum is adopted for the wave group generation. The spectrum and the amplitude of each wave component are expressed as

$$S(f_n) = \beta H_s^2 T_p^{-4} f_n^{-5}\exp\left[-\frac{5}{4}(T_p f_n)^{-4}\right]\gamma^{\exp\left[-(f_n/f_p-1)^2/2\sigma^2\right]}, \tag{14}$$

$$\beta = \frac{0.062\,38}{(0.23+0.0336\gamma) - 0.185(1.9+\gamma)^{-1}}[1.094 - 0.019\,15\ln(\gamma)], \tag{15}$$

$$A_n(f_n) = A_{in}\frac{S(f_n)\Delta f}{\sum S(f_n)\Delta f}, \tag{16}$$

where H_s denotes the significant wave height and T_p and f_p represent the peak wave period and frequency, respectively. The peak enhancement parameter γ is set to 3.30. The spectral width parameter σ is defined as $\sigma = 0.07$ for $\omega_n \le \omega_p$ and $\sigma = 0.09$ for $\omega_n > \omega_p$. The frequencies considered in this study range from $0.5f_p$ to $3.0f_p$, which covers most energy in the spectrum. A total of 2000 wave components are included in the focused wave group, thus a discrete frequency of $\Delta f = 0.000\,75 f_p$ is employed. The amplitude of the focused wave group, denoted as $A_{in} = \sum_{n=1}^{N} A_n$, represents the sum of all individual wave components A_n.

To simulate the propagation of different types of waves, the initial surface profiles must first be imposed as specified in Eq. (10). Different types of incident waves can be generated by applying the appropriate boundary conditions. It is noticeable that the wave generation method in the present model differs from the mechanical wavemaker used in physical tanks.

A mathematical absorber P_s is incorporated as a linear damping element in the free surface boundary condition outlined in Eq. (3) to attenuate reflected waves at the terminus of the numerical wave tank. The modified boundary condition is expressed as

$$\phi_t + \frac{1}{2}\left(\phi_x^2+\phi_y^2\right) + g\eta + P_S/\rho = 0 \quad \text{on} \quad y=\eta(x,t), \tag{17}$$

$$P_S/\rho = \varepsilon(x)\phi(x,\eta(x,t),t), \tag{18}$$

$$\varepsilon(x) = e^{-[(x-L_W)/2]^2}, \tag{19}$$

where L_W is the length of the damping layer, which is half the length of the numerical tank, and ρ is the fluid density. The choice of the damping function $\epsilon(x)$ can be changed depending on the region of data required.

III. MODEL VALIDATION

A. Convergence

As the fully nonlinear numerical models achieve the solution with the help of the Pseudo-spectral method, its convergence of the Fourier terms needs to be evaluated to ensure the accuracy of the numerical model. Convergence tests were carried out by simulating wave groups with varying numbers of discrete Fourier points per

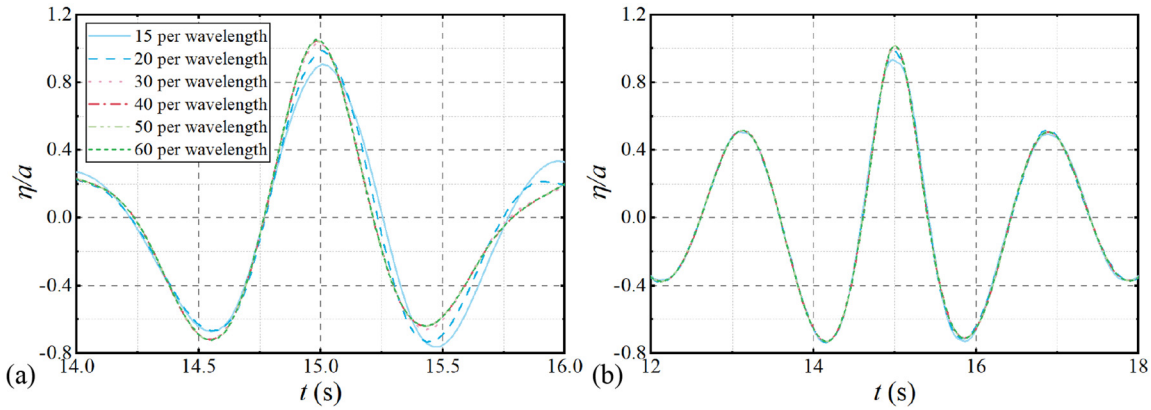

FIG. 2. Surface elevations of focused wave group at focusing with (a) the constant depth and (b) the 4 ripples.

wavelength. The wave profiles over different seabed configurations cover two cases,[25,48] specifically a horizontal seabed [Fig. 2(a)] and a rippled seabed [Fig. 2(b)], where the number of discrete points ranges from 15 to 60 per wavelength.

The results for both conditions indicate that focused wave profiles converge to near-identical values when the number of discrete Fourier points is higher than 30 per wavelength. A discrete Fourier resolution of 50 points per wavelength is deemed sufficient to accurately capture the nonlinear propagation of focused wave groups over both constant and varying depths. On the constant water depth, the focused wave profile remains symmetrical along the vertical direction, with smaller neighboring crests. In contrast, the introduction of ripples can alter wave dynamics. The ripples cause variations in local water depth, which decrease the wavelength and increase the neighboring crest. In addition, convergence tests of the fully nonlinear numerical model using conformal mapping methods have been conducted for different interplay conditions, including the monochromatic waves and focused wave groups, propagating over the non-step and step conditions.[40,49] Therefore, considering the accuracy of nonlinear effect capture when the wave is steep, 50 Fourier points per wavelength are employed for the simulations in this study.

B. Validation for Bragg resonance

To evaluate the capability of the present fully nonlinear numerical model in the study of Bragg resonance, the reflection coefficients of monochromatic waves were compared with previous studies.[19,22,25]

TABLE I. Bar parameters.

Case	D (m)	S (m)	M	h_0 (m)
D1	0.05	1.00	2	0.156
D2	0.05	1.00	4	0.156
D3	0.05	1.00	10	0.313

Ripples were commonly used in the literature to study Bragg resonance. In order to stimulate the Bragg resonance, Davies and Heathershaw[25] used regular waves over ripples in a series of tests, mostly using seabeds with four or ten ripples. Figure 3 shows a comparison of reflection coefficients for regular waves. The parameters of the periodic seabed are detailed in Table I. D and M denote the amplitude and number of ripples, respectively, while S represents the distance between two adjacent ripples. Note that the water depths h_0 differ in Cases D1 ($h_0 = 0.156$ m), D2 ($h_0 = 0.156$ m), and D3 ($h_0 = 0.313$ m). These case parameters will be adopted in the numerical simulations for the discussion of resonant coefficients.

In Fig. 3, the numerical results from the fully nonlinear model are contrasted with previous theoretical, experimental, and numerical results.[19,22,25] Case parameters for D2 and D3 are used in Figs. 3(a) and 3(b), respectively. The present model is well validated by the experimental and numerical results for the two types of ripples, D2

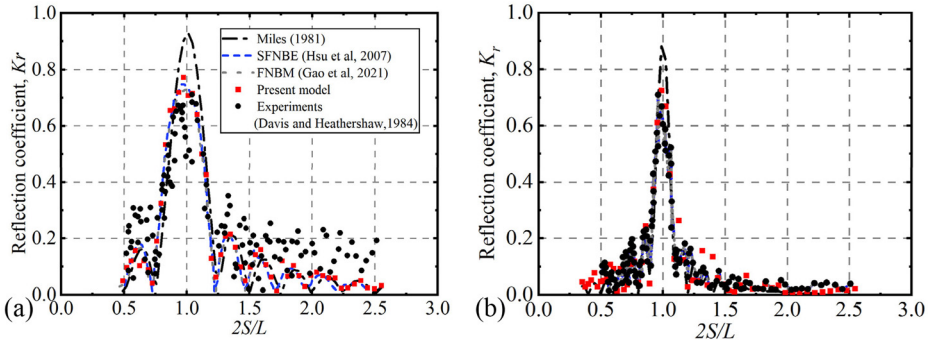

FIG. 3. Reflection coefficients of regular waves over the ripples: (a) $M = 4, h_0 = 0.156$ m (Case D2) and (b) $M = 10, h_0 = 0.313$ m (Case D3).

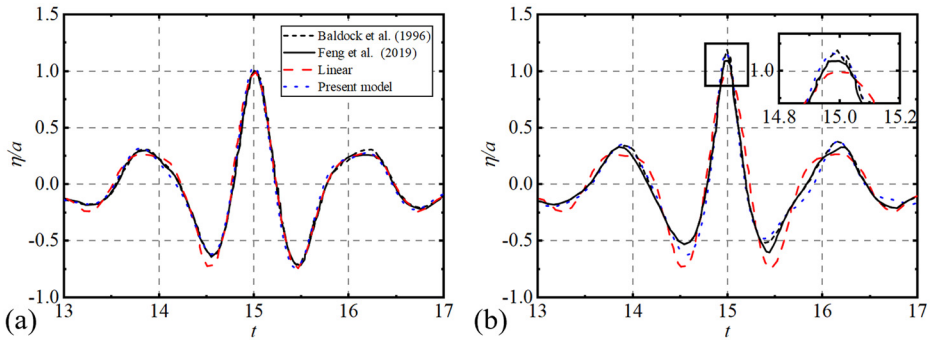

FIG. 4. Wave profiles of the focused wave group at the focused position for (a) $a = 0.022$ m and (b) $a = 0.055$ m.

and D3. It is observed that both the Bragg resonance and effective bandwidth of peak wave reflection are well captured using the present fully nonlinear model, where the bandwidth is the range of resonance frequencies with high reflection coefficients.[20] Since the frequency and crests are significant factors in a strong nonlinear wave group, the present model is well validated in terms of wave nonlinearity. In contrast, Mile's model is found to be insufficient to calculate the reflection coefficients in Case D2, where the peak is exaggerated to 0.92. The agreement between the present model and the FNBM and SFNBE results is excellent, with peaks around 0.78 in Fig. 3(a). This further demonstrates the capability of the present model in simulating the propagation of regular waves over varying topography, providing a solid foundation for further studies on the nonlinear propagation of focused wave groups.

C. Validation for focused wave groups

To further validate the present model for simulating focused wave groups, the simulated wave profiles are compared with the measured data from Baldock *et al.*[48] and the numerical results from Feng[41] by a fully nonlinear simulation, as shown in Fig. 4. In the experiments in Baldock *et al.*,[48] wave groups were generated within periods of 0.6 s $\leq T \leq$ 1.4 s using 29 monochromatic wave components, where the wave periods were evenly divided. The water depth was set at $h_0 = 0.7$ m, and two incident amplitudes of focused wave groups, $a = 0.022$ and 0.055 m, were employed.

To compare the focused wave groups with two different amplitudes, the surface elevations were normalized with the incident amplitudes. It is seen in Fig. 4(a) that all models well predict the wave elevation when the wave group is mild with $a = 0.022$ m. With $a = 0.055$ m, it was found that the higher incident amplitude induces higher peaks 1.2 of focused wave groups in Fig. 4(b). Meanwhile, no matter whether the peak is 1.2 or the neighboring peak 0.4, they are sharper than those with a smaller amplitude in Fig. 4(a), 1.0 for peaks and 0.32 for neighboring peaks. In addition, the trough in Fig. 4(b) is flatter, which also presents the higher nonlinearity of wave profiles. The linear results (NewWave theory) are found to under-predict the wave crest but over-predict the two troughs neighboring the crest. This is because the nonlinearity becomes significant with a steeper wave group as a result of more pronounced wave–wave interactions during the group evolution. The linear model cannot consider the nonlinear effect. The present numerical results reproduce the sharp crest and agree well with the measured and the nonlinear results from Feng.[41] This demonstrates that focused wave groups can be accurately simulated using the present numerical model.

IV. RESULTS AND DISCUSSION

A. Bragg reflection with a focused wave group over ripples

This section analyzes the impact of wave nonlinearity on Bragg reflection across a rippled seabed, taking into account different amplitudes of focused wave groups. The numerical tank utilized for this study is set to be sufficiently long (60 times the character wavelength of the group) to accommodate the nonlinear evolution of the wave group, as depicted in Fig. 5. The ripple bottom length is 10 m. The wave absorber is set at the far end. The incident wave group profile is prescribed according to the NewWave theory at the left side of the tank. As mentioned in Sec. I, studies have extensively explored the Bragg reflection with monochromatic waves, whereas the Bragg reflection under large wave groups has received limited attention. Therefore, in this context, focused wave group propagation over ripples is investigated.

1. Nonlinear effects

Bragg resonance is commonly studied by examining the reflection coefficients. Thus, defining the reflection coefficients of focused wave groups is necessary. Given that the wave group is generated from a spectrum, the reflection coefficient of a wave group can be defined as similar to the situation of irregular waves. Analogous to the response amplitude operator (RAO) definition for random sea states, the total reflection coefficient Kr for a wave group passing over a varying bottom is defined as follows:

$$Kr = \sqrt{\frac{\sum_{i=1}^{N} S(f_i)df \cdot R_i^2}{\sum_{i=1}^{N} S(f_i)df}}, \tag{20}$$

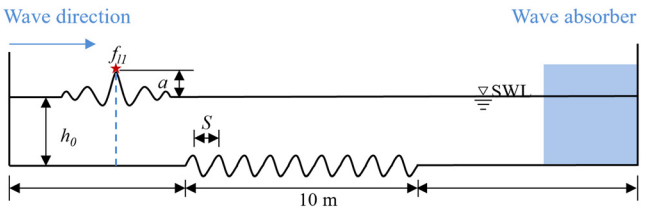

FIG. 5. Sketch of the numerical tank with ripples and location of focused positions $x_{f_{II}}$.

$$R_i = \frac{S_r(f_i)}{S_{in}(f_i)}, \tag{21}$$

where f_i denotes the frequency of each wave component in a wave group. R_i and $S(f_i)$ represent the corresponding reflection coefficient and the spectral density function for the ith frequency component. The subscripts "r" and "in" indicate reflected and incident focused waves, respectively. The reflected wave is defined as the difference between the surface elevation at varying water depths and a constant depth at the same location, with the location being 2.5 times the wavelength before the depth change. Note that the wave-topography interaction induces a downstream shift of focused position.[50] In this study, the selected position of reflected waves is set as 2.5 times the wavelength before the depth change, where the influence of the shift of focused wave position with nonlinear focused wave groups can be ignored. The surface elevations at the focused position on the constant water depth are utilized for the incident waves. Hence, for each case, configurations with and without the varying bottoms have been simulated.

Figure 6 illustrates the evolution of the focused wave group at the Bragg frequency, with a constant depth and a seabed featuring 10 ripples for Case D3. The time interval is 10 s from 5 to 65 s, and the shaded area represents the ripples. The water depth is $h_0 = 0.313$ m, and the incident wave group amplitude is $a = 0.015$ m. The wave group is focused at the time instant $t_{fl} = 16$ s and at the location $x_{f_{l1}} = 44$ m, which is 16 m in front of the ripples. As the focused wave group propagates over the rippled seabed at $t = 35$ s, a decrease in the crest, especially in the neighboring crests, is observed. Additionally, reflected waves are observed upstream. An attenuation of focused wave groups is evident from the profile that the crests of the wave group behind the ripples are reduced, compared with the constant water depth. To analyze the reflection behavior, the reflection coefficients for Case D3 are presented in Fig. 7. The relative wavelength $2S/L_P$ is varied by changing the peak wavelength L_P. Specifically, the wavelength of peak frequency is adjusted according to the incident peak frequency while keeping the spacing S constant. Results calculated using the theory of Miles[18] are included. To investigate the nonlinear effects, wave groups with varying steepnesses are compared. The peak Bragg reflection occurs around $2S/L_P = 1.0$, and the general agreement is satisfactory. Furthermore, as the incident amplitude a increases, a slight upshift in the corresponding Bragg frequency $2S/L_P$ is observed. Specifically, the case with $a = 0.050$ m exhibits the lowest peak reflection coefficient of 0.33 and the highest resonant $2S/L_P$ value of 1.06. As the wave amplitude increases, the nonlinear interactions cause a modification in the wave profile, which, in turn, affects the resonance condition. This shift is consistent with findings in previous studies, such as those by Peng *et al.*[7] and Guo *et al.*,[51] which also reported similar upshifts due to free surface nonlinearity.

The nonlinear focused wave profiles at the resonant frequency ($f_p = 0.767$ Hz) with different amplitudes at three time instants for Case D3 are presented in Fig. 8. The horizontal axis represents the

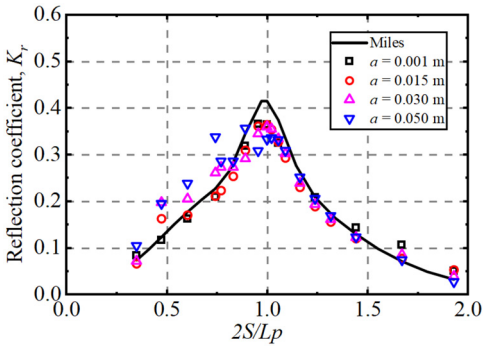

FIG. 7. Reflection coefficients of focused wave groups with varying incident amplitudes over 10 ripples (Case D3).

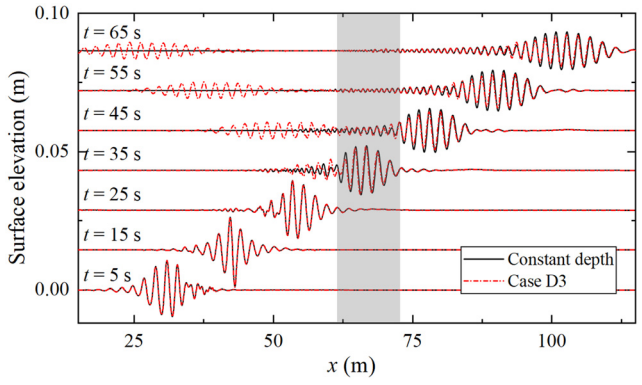

FIG. 6. Propagation of focused wave group over 10 ripples (Case D3) with $a = 0.015$ m.

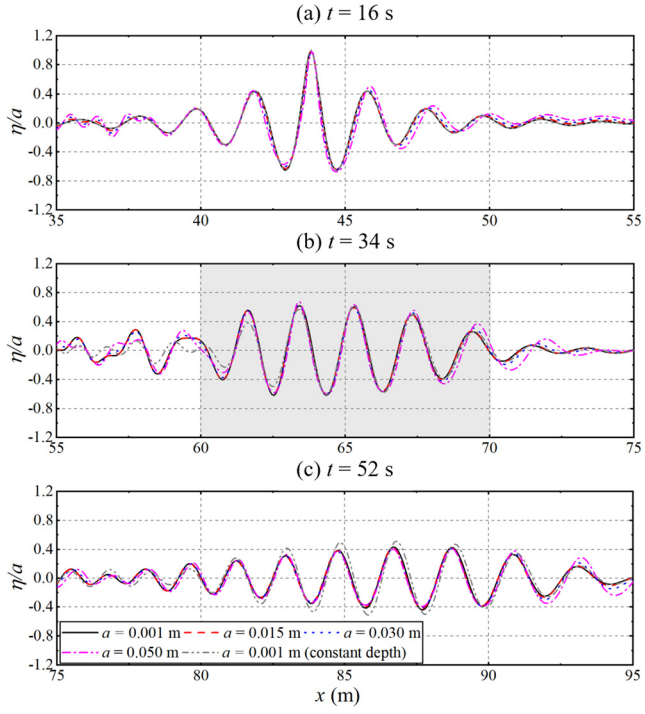

FIG. 8. Focused wave group in the spatial domain over 10 ripples (Case D3) at (a) $t = 16$ s, (b) $t = 34$ s, and (c) $t = 52$ s at $f_p = 0.767$ Hz.

distance to the wavemaker, and the vertical axis denotes the nondimensional surface wave elevation, divided by the corresponding incident wave amplitude a. The three time instants correspond to the focused time, the occurrence of maximum elevations over ripples, and a time when the focused wave passed the ripples. Notably, the peak elevations occur at the focused time ($t_{fl} = 16$ s) and at the focused position ($x_{fl} = 44$ m). As the amplitude increases to $a = 0.050$ m, a clear asymmetry emerges in the wave profile. At $t = 34$ s, the maximum normalized elevation over the ripples [shaded area in Fig. 8(b)] reaches approximately 0.67, which is less than the elevation at the focused time. Comparison of these normalized peaks with those in constant water depth ($a = 0.001$ m) reveals that obvious modification of the wave profiles in front of and behind the ripple regions is observed. However, when the focused wave group propagates past the ripples at $t = 52$ s, the maximum elevation drops to 0.42, whereas the normalized crest of the focused wave group is 0.51 in the constant depth. This indicates that the ripples can effectively attenuate the wave groups, but the nonlinear effect is less significant behind the ripple region from the transmitted waves. Overall, the incident and transmitted wave profiles remain similar across varying amplitudes.

To further investigate the nonlinear effects of the wave amplitudes, the energy spectra of the incident and transmitted waves for Case D3 are displayed in Fig. 9. The surface elevations were normalized with the incident amplitude to facilitate comparison between spectra of waves with varying amplitudes. Upon examination of incident focused wave groups at the focused position in Fig. 9(a), discrepancies are observed in the tails of the incident spectra ($f/f_p > 1.6$). Higher amplitudes induce stronger nonlinearity, which primarily manifests in the enhancement of subharmonics ($f/f_p = 0$–0.5) and superharmonics ($f/f_p = 1.5$–2.5). The occurrence of sub- and superharmonics is due to the interaction of each harmonic, leading to the sum and difference of wave energy. Additionally, an increase in wave group amplitude leads to a higher spectral tail for both incident and the transmitted waves. Notably, a reduction in wave components at the fundamental frequency is observed in Fig. 9(b). This might show possible energy transfer among different frequency harmonics as a result of nonlinear effects.

B. Bragg resonance with three bottom configurations

To study the effect of different seabed configurations on resonant reflection, three types of seabed configurations are employed: ripples, rectified cosinoidal bars, and steps, as illustrated in Fig. 10. The rectified cosinoidal bars are half the horizontal length of the ripples. The steps are rectangular bars with sharp corners. The effects of the number of bars or steps (M), spacing (S), and seabed height (D) on Bragg resonance are studied numerically.

1. Wave reflection by three types of seabed configurations

Existing studies have primarily focused on Bragg resonance with seabed configurations of ripples subjected to regular waves.[19,24,32] In this study, the effects of rectified cosinoidal bars and steps subject to focused wave groups are simulated. The amplitude of a near-linear focused wave groups is set to $a = 0.015$ m, with $h_0 = 0.156$ m. Figures 11 and 12 display the reflection coefficients for the three types of seabed configurations in Cases D2 and D3, respectively. It is seen that Bragg resonance is observed in all cases, with peak K_r at $2S/L_P = 1.0$. In Fig. 11, the frequency bandwidth of Bragg reflection is broadest with ripples, whereas the reflection coefficients with steps are slightly higher than those with rectified cosinoidal bars. It is notable that the reflection coefficients for ripples are the highest at the relative wavelength $2S/L_P = 1.0$. Then, the reflection coefficients with three bottom configurations converge at around $2S/L_P = 1.5$. When $2S/L_P$ is greater than 1.5, the reflection coefficients for ripples are reduced to be the lowest. A similar phenomenon is observed in deeper water depths ($h_0 = 0.313$ m) as seen in Case D3 (Fig. 12). The peak reflections for ripples ($K_r = 0.38$) are higher than those for rectified cosinoidal bars ($K_r = 0.23$) and steps ($K_r = 0.30$). Then, the reflection coefficients gradually become equal at $2S/L_P = 1.6$. Finally, the increase in $2S/L_P$ leads to the trend that the reflection coefficient for the step configuration becomes higher than that of the other two bottom configurations. The ripple configuration results in the highest reflection coefficients at $2S/L_P = 1.0$, while the step configuration provides better reflection for $2S/L_P > 2.0$. In consequence, to achieve the fundamental and second order Resonance peaks, different seabed configurations exhibit different excitation conditions.

2. Shift of second order Bragg resonance frequency

For each type of seabed configuration, the effects of the number of bars are studied for $M = 2, 4, 10$ at a water depth of $h_0 = 0.156$ m. Figure 13 displays the reflection coefficients for ripples and rectified cosinoidal bars. It is found that the resonant peaks increase with the number of bars. For instance, the resonant peak ($K_r = 0.39$) with 4

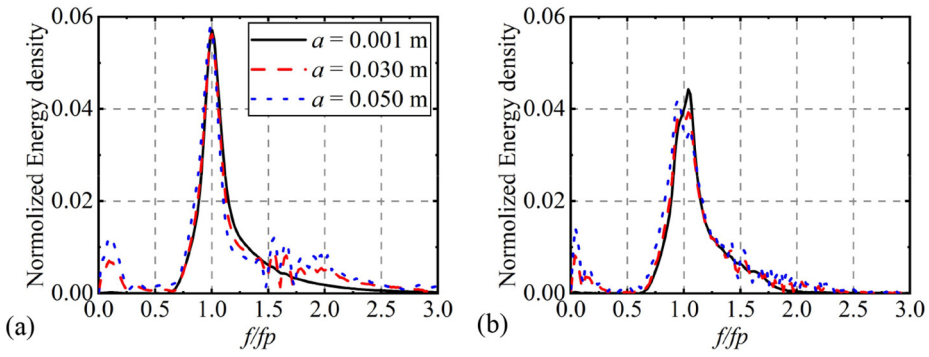

FIG. 9. Normalized wave energy spectra over 10 ripples (Case D3) with (a) the incident waves and (b) the transmitted waves.

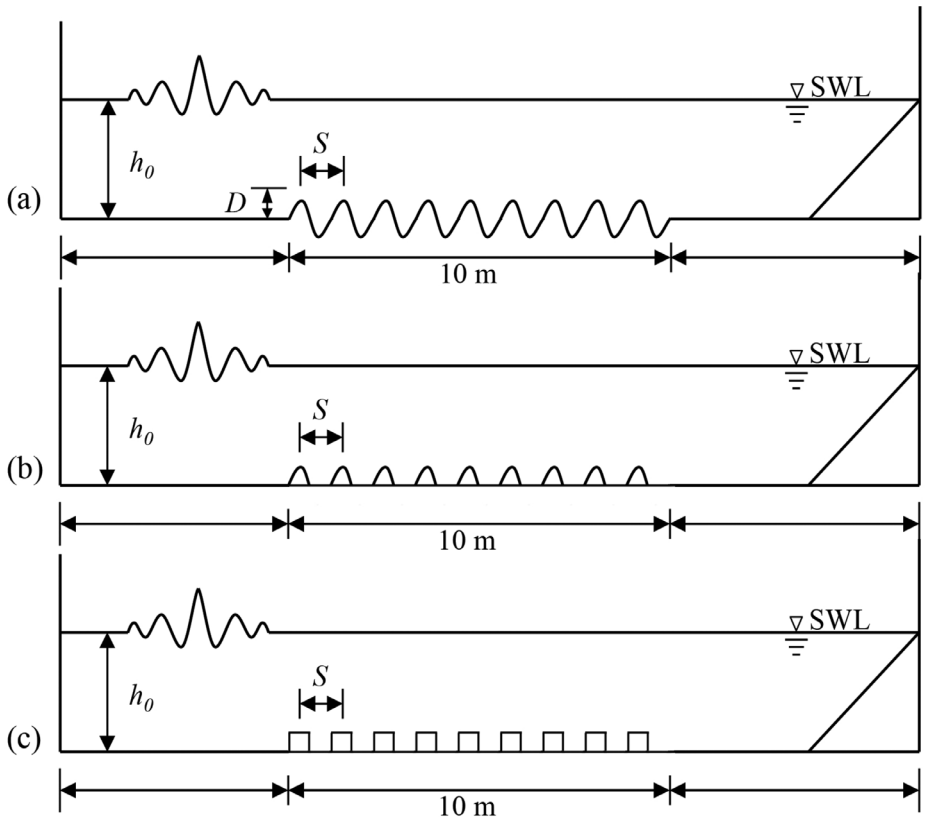

FIG. 10. Three types of seabed configurations: the ripples, rectified cosinoidal bars, and submerged steps with $D = 0.05$ m, $S = 1.0$ m, and $M = 10$ (Case D3): (a) ripples, (b) rectified cosinoidal bars, and (c) steps.

rectified cosinoidal bars is 1.5 times higher than that ($K_r = 0.22$) with 2 rectified cosinoidal bars. Additionally, the corresponding bandwidth of Bragg resonance (frequency range of high reflection) is observed to become broader.

Apart from the fundamental Bragg resonance peak at $2S/L_P = 1.0$, a second peak is observed in the cases with rectified cosinoidal bars in Fig. 13(b). This corresponds to a second order Bragg resonance at $2S/L_P = 2.0$. The wavelength L_P at the second order Bragg resonance is half of the peak wavelength at the fundamental Bragg resonance. The second order Bragg resonance is excited by the strong interaction between focused wave groups and the periodic rectified cosinoidal bars. The peaks of the second order Bragg resonance are approximately half of those of the fundamental Bragg resonance. The second order Bragg resonance seems more obvious with the increase in the number of bars, explained by stronger interactions between the wave group and the rectified bars.

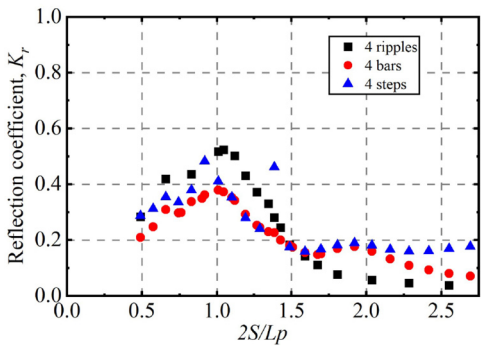

FIG. 11. Reflection coefficients over three types of seabed configurations with the incident amplitude $a = 0.015$ m and frequency range $(0.5 - 3.0)f_p$, $M = 4$ (Case D2).

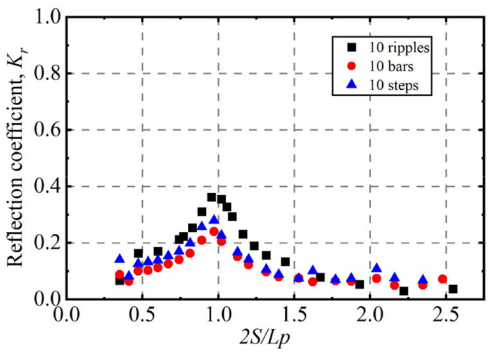

FIG. 12. Reflection coefficients over three types of seabed configurations with the incident amplitude $a = 0.015$ m and frequency range $(0.5 - 3.0)f_p$, $M = 10$ (Case D3).

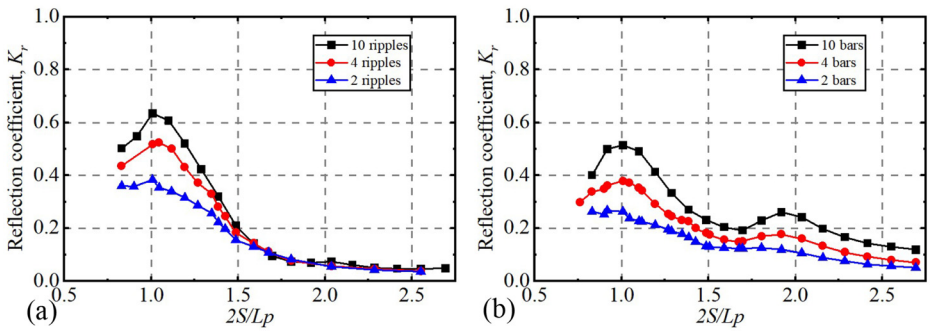

FIG. 13. Reflection coefficients over seabed with the incident amplitude $a = 0.015$ m, $h_0 = 0.156$ m, and frequency range $(0.5 - 3.0)f_p$: (a) ripples and (b) rectified cosinoidal bars.

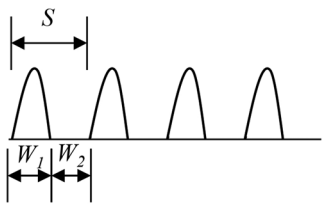

FIG. 14. Sketch of the width (W_1, W_2) with W_1 being the length of bars and W_2 being the length of a flat area.

3. Configuration of the bars

In addition, the effects of spacing S and widths (W_1, W_2) are examined. These parameters denote the bar width and gap width. Section IV A discusses Bragg resonance over ripples, and the spacing S was set to 1.0 m, with specific widths $W_1 = 0.5$ m and $W_2 = 0.5$ m, as illustrated in Fig. 14. This section investigates the reflection coefficients with variations in both the spacing and width of rectified cosinoidal bars and steps. Figure 15 illustrates cases with $M = 4$ (Case D2), and Fig. 16 shows cases with $M = 10$ (Case D3). Three combinations of spacing and width for the bars are considered: $(W_1 = 0.5, W_2 = 0.5)$, $(W_1 = 0.6, W_2 = 0.4)$, and $(W_1 = 0.5, W_2 = 0.4)$. For Case D2, the highest peaks are observed in the group with $(W_1 = 0.6, W_2 = 0.4)$, with reflection coefficients reaching $K_r = 0.38$ for rectified cosinoidal bars. For periodic steps, the resonant peak with $(W_1 = 0.6, W_2 = 0.4)$ reaches nearly 0.5, representing a clear increase compared to 0.43 in the case with $(W_1 = 0.5, W_2 = 0.5)$. A relative upshifting of the wavelength is observed for all three combinations of spacing and width of rectified cosinoidal bars. The excitation condition for fundamental Bragg resonance, $2S/L_P$, is approximately 1.0 for $(W_1 = 0.5, W_2 = 0.5)$ and

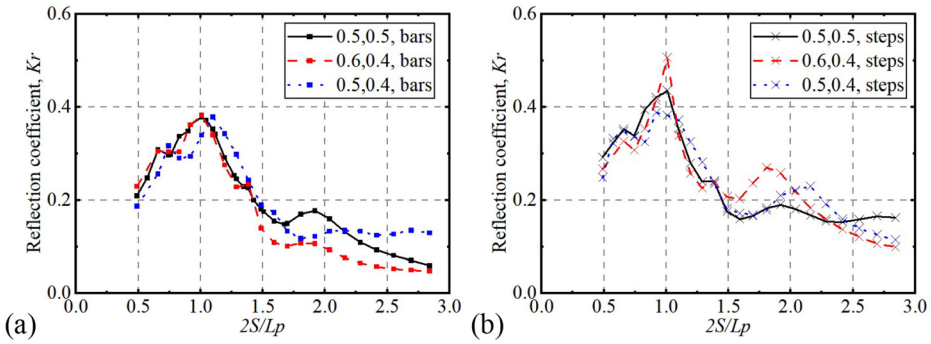

FIG. 15. Reflection coefficients with different groups of spacing and width with the incident amplitude $a = 0.015$ m and frequency range $(0.5 - 3.0)f_p$: (a) $M = 4$, $h_0 = 0.156$ m, rectified cosinoidal bars, and (b) $M = 4$, $h_0 = 0.156$ m, steps.

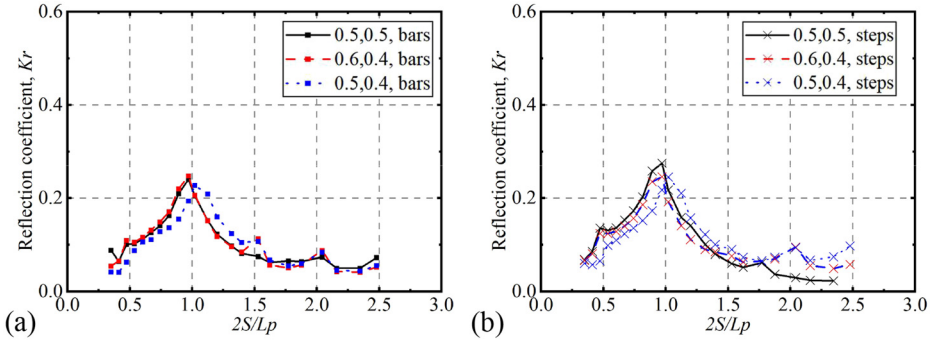

FIG. 16. Reflection coefficients with different groups of spacing and width with the incident amplitude $a = 0.015$ m and frequency range $(0.5 - 3.0)f_p$: (a) $M = 10$, $h_0 = 0.313$ m, rectified cosinoidal bars and (b) $M = 10$, $h_0 = 0.313$ m, steps.

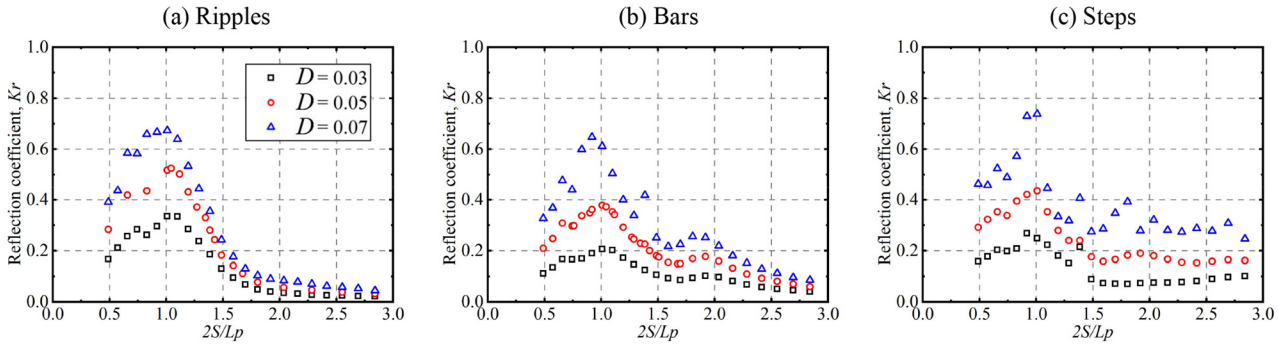

FIG. 17. Reflection coefficients with different heights for rectified cosinoidal bars and steps with the incident amplitude $a = 0.015$ m and frequency range $(0.5 - 3.0)f_p$, $M = 4$ (Case D2): (a) ripples, (b) bars, and (c) steps.

$(W_1 = 0.6, W_2 = 0.4)$ but shifts to 1.1 for $(W_1 = 0.5, W_2 = 0.4)$. For the second order Bragg resonance with $(W_1 = 0.6, W_2 = 0.4)$, the condition for rectified cosinoidal bars is $2S/L_P = 1.9$, while for steps, it is $2S/L_P = 1.8$. This indicates a downshift in the dimensionless parameter $2S/L_P$ for both types of periodic bars. Additionally, for both rectified cosinoidal bars and steps, the value of $2S/L_P$ increases to 2.2 with $(W_1 = 0.5, W_2 = 0.4)$. The variations in reflection coefficients attributable to W_1 and W_2 are consistent with the findings of Liu *et al.*[15] (2019), who posited that bar width and spacing exert a relatively minor influence compared to other factors such as bar height and number. Notwithstanding their subtle nature, these parameters can, indeed, modulate Bragg resonance characteristics, particularly in terms of peak reflection coefficients and resonance bandwidth.

For the deeper water depth h_0 (Case D3) illustrated in Fig. 16, the deviations among the second order Bragg resonances are negligible. Discrepancies among the three groups remain small for both 10 rectified cosinoidal bars and steps. The peak reflection coefficient, at 0.28, is highest for steps with $(W_1 = 0.5, W_2 = 0.5)$. Meanwhile, the second order Bragg reflection coefficient peaks for the latter two groups are identical. In a shallower water depth, variations in width and spacing significantly influence excitation conditions, especially for the second order Bragg resonance. However, an increased water depth h_0 for Case D3 can mitigate the differences induced by variations in spacing and widths.

4. Influence of the height of seabed

Apart from the number and spacing, the height of the seabed D also serves as an important factor influencing the Bragg resonant peaks.[52] Figure 17 displays the reflection coefficients for different heights $D = 0.03$ m, $D = 0.05$ m, and $D = 0.07$ m for seabeds consisting of ripples, rectified cosinoidal bars, and steps with $M = 4$ (Case D2). It was observed an increase in the reflection peaks with the rise in seabed height. To provide a more quantitative insight, we have calculated the percentage increase in the reflection coefficients when the seabed height is raised from 0.03 to 0.07 m. For the case with ripples, the reflection coefficient increases from approximately 0.36 to 0.68, which corresponds to an 89% increase. For rectified cosinoidal bars, the reflection coefficient increases from approximately 0.20 to 0.66, indicating a 230% increase. Finally, for steps, the reflection coefficient rises from approximately 0.25 to 0.78, showing a 212% increase. These quantitative insights highlight the sensitivity of Bragg resonance to changes in seabed height, providing a clearer understanding of the impact of seabed configurations on wave reflection. Figure 18 shows the results for $M = 10$ (Case D3). Cases with $D = 0.07$ m consistently exhibit the highest resonant peaks. For Case D3 with ripples, the peaks of the fundamental Bragg resonance increase approximately by 0.1 with every increment of 0.02 m in height. In addition, the peaks at $2S/L_P = 2.0$ are prominent in cases with $D = 0.07$ m. In cases with rectified cosinoidal bars and steps, the peaks at $2S/L_P = 2.0$ even

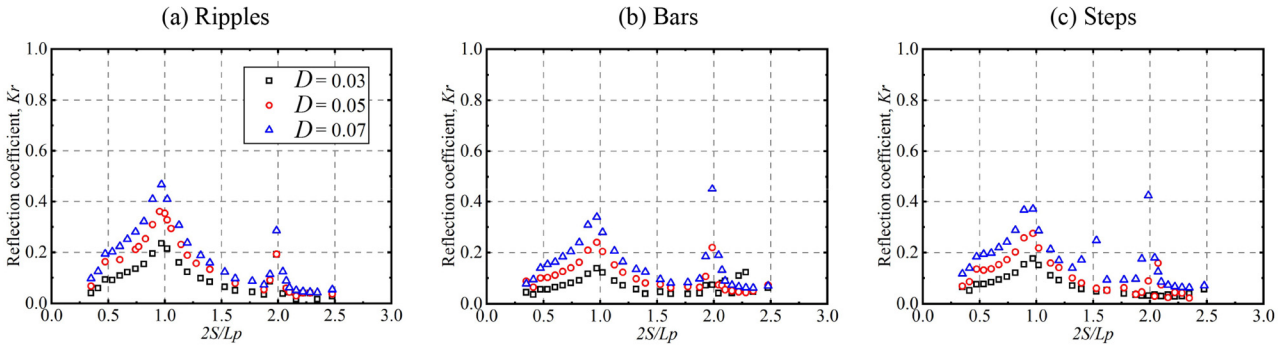

FIG. 18. Reflection coefficients with different heights for rectified cosinoidal bars and steps with the incident amplitude $a = 0.015$ m and frequency range $(0.5 - 3.0)f_p$, $M = 10$ (Case D3): (a) ripples, (b) bars, and (c) steps.

exceed those of the fundamental Bragg reflection as seabed height increases. One potential explanation is that the depth changes induce the superharmonics, which are enhanced at the depth transitions.[43] This enhancement results in higher reflected waves, consequently increasing the superharmonics of the reflected waves, thereby exciting a second order Bragg resonance. The magnitude of the second order Bragg reflection may exceed that of the fundamental Bragg reflection, with potentially exceeding the fundamental reflection coefficients by up to 20% at greater bar heights. In summary, increasing the bar height effectively enlarges the Bragg resonance peaks. The shift in the dimensionless parameter $2S/L_P$ is small in this context.

V. CONCLUSIONS

This study presents a fully nonlinear numerical model using the conformal mapping technique to study the Bragg resonance of focused wave groups over periodic seabed topography. Validation against experimental, theoretical, and numerical results confirms the model's accuracy. This study demonstrates that increased wave amplitudes or steepnesses slightly shift the corresponding resonant wavelength $2S/L_P$. Specifically, the peak Bragg reflection for a wave group with an amplitude of 0.050 m occurs at $2S/L_P = 1.06$, compared to $2S/L_P = 1.0$ for a wave group with an amplitude of 0.015 m. Higher wave steepnesses result in increased subharmonics and superharmonics, enhancing the complexity of wave interactions.

Three types of periodic seabed are considered: ripples, rectified cosinoidal bars, and steps. The ripples configuration resulted in the highest reflection coefficients at $2S/L_P = 1.0$, with a peak reflection coefficient of 0.38, while the step configuration provided better reflection for $2S/L_P > 2.0$. Increasing the number of bars significantly enhances wave reflection, with the reflection coefficient for 10 rectified cosinoidal bars being 1.5 times higher than that for 2 bars. The effects of seabed bar spacing, width, and height were also studied. Proper bar spacing and width can optimize Bragg reflection, particularly when fewer bars are present. Increasing the seabed height remarkably amplifies reflection coefficients, potentially inducing a second order Bragg reflection that may exceed the fundamental one.

These findings provide valuable insights into the nonlinear interactions between focused wave groups and periodic seabeds, which are crucial for designing effective coastal protection structures. The results highlight the importance of considering both wave parameters and seabed configurations in coastal engineering applications. Nevertheless, further detailed investigations of the characteristics of the subharmonics and superharmonics triggered by the periodic seabeds are needed at Bragg resonance, given focused wave groups can be strongly nonlinear.

ACKNOWLEDGMENTS

The author X. Feng is grateful for the support of the National Key Research and Development Program of China (Grant No. 2023YFB3711500) and the Shenzhen Science and Technology Program (KCXST20221021111409023). Y. Dong is grateful for the support of the Research Grants Council of the Hong Kong Special Administrative Region, China (No. PolyU 15225722).

AUTHOR DECLARATIONS

Conflict of Interest

The authors have no conflicts to disclose.

Author Contributions

Qian Wu: Data curation (equal); Formal analysis (equal); Investigation (equal); Methodology (equal); Validation (equal); Visualization (equal); Writing – original draft (equal). **Xingya Feng**: Conceptualization (equal); Formal analysis (equal); Funding acquisition (equal); Investigation (equal); Methodology (equal); Project administration (equal); Resources (equal); Supervision (equal); Writing – review & editing (equal) **You Dong:** Formal analysis (equal); Investigation (equal); Validation (equal); Writing – review & editing (equal).

DATA AVAILABILITY

The data that support the findings of this study are available within the article.

REFERENCES

[1]M. Belzons, V. Rey, and E. Guazzelli, "Subharmonic Bragg resonance for surface water waves," Europhys. Lett. **16**, 189 (1991).
[2]T.-W. Hsu, L.-H. Tsai, and Y.-T. Huang, "Bragg scattering of water waves by multiply composite artificial bars," Coastal Eng. J. **45**, 235–253 (2003).
[3]W. Liu, Y. Liu, and X. Zhao, "Numerical study of Bragg reflection of regular water waves over fringing reefs based on a Boussinesq model," Ocean Eng. **190**, 106415 (2019).
[4]Y. Liu, H.-J. Li, and L. Zhu, "Bragg reflection of water waves by multiple submerged semi-circular breakwaters," Appl. Ocean Res. **56**, 67–78 (2016).
[5]L.-H. Tsai, Y.-S. Kuo, Y.-J. Lan, T.-W. Hsu, and W.-J. Chen, "Investigation of multiply composite artificial bars for Bragg scattering of water waves," Coastal Eng. J. **53**, 521–548 (2011).
[6]J. Xu, L. Chen, D. Ning, and M. Zhao, "Resonance of water waves propagating over a uniform and a graded line array of rectified submerged cosinoidal bars," Appl. Ocean Res. **134**, 103531 (2023).
[7]J. Peng, A. Tao, Y. Liu, J. Zheng, J. Zhang, and R. Wang, "A laboratory study of class III Bragg resonance of gravity surface waves by periodic beds," Phys. Fluids **31**, 067110 (2019).
[8]S. Zhang, L. Chen, D. Ning, and B. Teng, "Multi-Bragg reflections over a periodic submerged structure," in Proceedings of the 36th International Workshop on Water Waves and Floating Bodies, Seoul, Korea, 25–28 April, 2021.
[9]D. Ning, S. Zhang, L. Chen, H.-W. Liu, and B. Teng, "Nonlinear Bragg scattering of surface waves over a two-dimensional periodic structure," J. Fluid Mech. **946**, A25 (2022a).
[10]H. Zhang, A. Tao, J. Tu, J. Su, and S. Xie, "The focusing waves induced by Bragg resonance with V-shaped undulating bottom," J. Mar. Sci. Eng. **9**, 708 (2021).
[11]E. Didenkulova, I. Didenkulova, and I. Medvedev, "Freak wave events in 2005–2021: Statistics and analysis of favourable wave and wind conditions," Nat. Hazards Earth Syst. Sci. **23**, 1653–1663 (2023).
[12]J. T. Kirby and J. P. Anton, "Bragg reflection of waves by artificial bars," In Coastal Eng. 757–768 (1990).
[13]H.-W. Liu, Y.-P. Shi, and D.-Q. Cao, "Optimization of parabolic bars for maximum Bragg resonant reflection of long waves," J. Hydrodyn. **27**, 373–382 (2015).
[14]H. Zeng, B. Qin, and J. Zhang, "Optimal collocation of Bragg breakwaters with rectangular bars on sloping seabed for Bragg resonant reflection by long waves," Ocean Eng. **130**, 156–165 (2017).
[15]H.-W. Liu, Y. Liu, and P. Lin, "Bloch band gap of shallow-water waves over infinite arrays of parabolic bars and rectified cosinoidal bars and Bragg resonance over finite arrays of bars," Ocean Eng. **188**, 106235 (2019).

[16]J.-J. Xie and H.-W. Liu, "Analytical study of Bragg resonances by a finite periodic array of congruent trapezoidal bars or trenches on a sloping seabed," Appl. Math. Modell. **119**, 717–735 (2023).
[17]C.-H. Jeon and Y.-S. Cho, "Bragg reflection of sinusoidal waves due to trapezoidal submerged breakwaters," Ocean Eng. **33**, 2067–2082 (2006).
[18]J. W. Miles, "Oblique surface-wave diffraction by a cylindrical obstacle," Dyn. Atmos. Oceans **6**, 121–123 (1981).
[19]J. Gao, X. Ma, G. Dong, H. Chen, Q. Liu, and J. Zang, "Investigation on the effects of Bragg reflection on harbor oscillations," Coastal Eng. **170**, 103977 (2021).
[20]F. Ardhuin and T. Herbers, "Bragg scattering of random surface gravity waves by irregular seabed topography," J. Fluid Mech. **451**, 1–33 (2002).
[21]C. Lee, G. Kim, and K.-D. Suh, "Extended mild-slope equation for random waves," Coastal Eng. **48**, 277–287 (2003).
[22]T.-W. Hsu, S.-C. Hsiao, S.-H. Ou, S.-K. Wang, B.-D. Yang, and S.-E. Chou, "An application of Boussinesq equations to Bragg reflection of irregular waves," Ocean Eng. **34**, 870–883 (2007).
[23]A. Abbasnia, M. Ghiasi, and A. H. Abbasnia, "Irregular wave transmission on bottom bumps using fully nonlinear NURBS numerical wave tank," Eng. Anal. Boundary Elem. **82**, 130–140 (2017).
[24]K. D. Suh, C. Lee, and W. S. Park, "Time-dependent equations for wave propagation on rapidly varying topography," Coastal Eng. **32**, 91–117 (1997).
[25]A. Davies and A. Heathershaw, "Surface-wave propagation over sinusoidally varying topography," J. Fluid Mech. **144**, 419–443 (1984).
[26]P. L.-F. Liu and Y.-S. Cho, "Bragg reflection of infragravity waves by sandbars," J. Geophys. Res.: Oceans **98**, 22733–22741, https://doi.org/10.1029/93JC02350 (1993).
[27]Y.-S. Cho and J.-S. Jung, "Bragg resonant reflection of carrier waves composing wave groups," Ocean Eng. **33**, 82–92 (2006).
[28]J. Gao, L. Hou, Y. Liu, and H. Shi, "Influences of Bragg reflection on harbor resonance triggered by irregular wave groups," Ocean Eng. **305**, 117941 (2024).
[29]H. Fernández, V. Sriram, S. Schimmels, and H. Oumeraci, "Extreme wave generation using self correcting method—Revisited," Coastal Eng. **93**, 15–31 (2014).
[30]R. Moideen and M. R. Behera, "Numerical investigation of extreme wave impact on coastal bridge deck using focused waves," Ocean Eng. **234**, 109227 (2021).
[31]F. Zeng, N. Zhang, G. Huang, Q. Gu, and W. Pan, "A novel method in generating freak wave and modulating wave profile," Mar. Struct. **82**, 103148 (2022).
[32]D. Ning, C. Liang, L. Chen, and C. Zhang, "Numerical investigation on the propagation and evolution of focused waves over a sloping bed," Ocean Eng. **250**, 111035 (2022b).
[33]E. Guazzelli, V. Rey, and M. Belzons, "Higher-order Bragg reflection of gravity surface waves by periodic beds," J. Fluid Mech. **245**, 301–317 (1992).
[34]Y. Ding, H.-W. Liu, and P. Lin, "Quantitative Expression of the Modified Bragg's Law for Bragg resonances of water waves excited by five types of artificial bars," Phys. Fluids **36**, 047130 (2024).
[35]H.-W. Liu, "An approximate law of Class I Bragg resonance of linear shallow-water waves excited by five types of artificial bars," Ocean Eng. **267**, 113245 (2023).
[36]H.-W. Liu, W. Xiong, and J.-J. Xie, "A new law of Class I Bragg resonance for linear long waves over arrays of parabolic trenches or rectified cosinoidal trenches," Ocean Eng. **281**, 114973 (2023).
[37]X. Feng and W. Bai, "Wave resonances in a narrow gap between two barges using fully nonlinear numerical simulation," Appl. Ocean Res. **50**, 119–129 (2015).
[38]D. Clamond and J. Grue, "A fast method for fully nonlinear water-wave computations," J. Fluid Mech. **447**, 337–355 (2001).
[39]C. Viotti, D. Dutykh, and F. Dias, "The conformal-mapping method for surface gravity waves in the presence of variable bathymetry and mean current," Procedia IUTAM **11**, 110–118 (2014).
[40]Q. Wu, X. Feng, Y. Dong, and F. Dias, "On the behavior of higher harmonics in the evolution of nonlinear water waves in the presence of abrupt depth transitions," Phys. Fluids **35**, 127102 (2023).
[41]X. Feng, "Analysis of higher harmonics in a focused water wave group by a nonlinear potential flow model," Ocean Eng. **193**, 106581 (2019).
[42]L. Wang, J. X. Li, S. X. Liu, and Y. P. Fan, "Experimental and numerical studies on the focused waves generated by double wave groups," Front. Energy Res. **8**, 133 (2020).
[43]Y. Li, Y. Zheng, Z. Lin, T. A. Adcock, and T. S. van den Bremer, "Surface wave-packets subject to an abrupt depth change. Part 1. Second-order theory," J. Fluid Mech. **915**, A71 (2021).
[44]M. Onorato, A. R. Osborne, M. Serio, L. Cavaleri, C. Brandini, and C. T. Stansberg, "Extreme waves, modulational instability and second order theory: Wave flume experiments on irregular waves," Eur. J. Mech. B. Fluids **25**, 586–601 (2006).
[45]E. J. Ransley, S. A. Brown, M. Hann, D. M. Greaves, C. Windt, J. Ringwood, J. Davidson, P. Schmitt, S. Yan, J. X. Wang *et al.*, "Focused wave interactions with floating structures: A blind comparative study," Proc. Inst. Civ. Eng. Eng. Comput. Mech. **174**, 46–61 (2021).
[46]R. J. Rapp and W. K. Melville, "Laboratory measurements of deep-water breaking waves," Philos. Trans. R. Soc. London, Ser. A **331**, 735–800 (1990).
[47]V. Sriram, T. Schlurmann, and S. Schimmels, "Focused wave evolution using linear and second order wavemaker theory," Appl. Ocean Res. **53**, 279–296 (2015).
[48]T. E. Baldock, C. Swan, and P. H. Taylor, "A laboratory study of nonlinear surface waves on water," Philos. Trans. R. Soc. London, Ser. A **354**, 649–676 (1996).
[49]Q. Wu, X. Feng, and Y. Dong, "Nonlinear computation for focused wave groups on abrupt depth transitions," IOP Conf. Ser.: Mater. Sci. Eng. **1288**, 012011 (2023).
[50]D. Ning, J. Zang, S. Liu, R. E. Taylor, B. Teng, and P. Taylor, "Free-surface evolution and wave kinematics for nonlinear uni-directional focused wave groups," Ocean Eng. **36**, 1226–1243 (2009).
[51]F.-C. Guo, H.-W. Liu, and J.-J. Pan, "Phase downshift or upshift of Bragg resonance for water wave reflection by an array of cycloidal bars or trenches," Wave Motion **106**, 102794 (2021).
[52]H.-K. Chang and J.-C. Liou, "Long wave reflection from submerged trapezoidal breakwaters," Ocean Eng. **34**, 185–191 (2007).